Pure Appl. Chem., Vol. 81, No. 11, pp. 2093–2105, 2009.
doi:10.1351/PAC-CON-08-11-18

Effect of ozone on the structure and physicochemical properties of ultradisperse diamond and shungite nanocarbon elements*

Natalia N. Rozhkova[1,‡], Lyubov' E. Gorlenko[2], Galina I. Emel'yanova[2], Anna Jankowska[3], Michail V. Korobov[2], Valery V. Lunin[2], and Eiji Ōsawa[4]

[1]Institute of Geology, Karelian Research Centre, RAS, Petrozavodsk 185910, Russia; [2]Department of Chemistry, Moscow State University, Moscow 119991, Russia; [3]Institute of Chemistry and Technology of Petroleum and Coal, Wrocław University of Technology, 50-344 Wrocław, Poland; [4]NanoCarbon Research Institute, Asama Research Extension Centre, Shinshu University, 3-15-1 Tokita, Ueda, Nagano 386-8567, Japan

Abstract: A comparative study of the effect of ozonization on the physicochemical properties of naturally and synthetically generated nanocarbon materials, shungite carbon (ShC) and ultradisperse diamond (UDD) after special treatment in the form of monodisperse single nanodiamond particulates (*mdsn*-D), that have a similar two-level structural pattern (hierarchical system structure) and curved graphene shells or their fragments contribute to the formation of the structure and surface properties of both ShC and *mdsn*-D particles, was conducted.

The ozonization kinetics of ShC and *mdsn*-D showed their high catalytic activity during ozone decomposition. Upon ozonization, the graphene shell is removed selectively from the surface of the diamond core of *mdsn*-D, as shown by Fourier transform-infrared (FT-IR) spectroscopy and derivatography data. A distinctive characteristic of ShC is a substantial change in structural parameters upon ozonization: structural porosity increases and the size of coherent scatter domains decreases in the direction perpendicular to graphene layers [as shown by small-angle X-ray scattering (SAXS), transmission electron microscopy (TEM), and selected area electron diffraction (SAED) data], which agrees with adsorption experiments that showed an increase in ultramicroporosity and mesoporosity upon ozonization of ShC. The molecular probe technique was used to monitor changes in microporosity of ShC and *mdsn*-D.

Keywords: graphene elements; ozonization; porosity; shungite; ultradisperse diamond.

INTRODUCTION

Materials based on nanodimensional carbon particles are typically very strong and durable; all physicochemical processes, such as mass and heat exchange, etc., proceed faster on particles with a well-developed surface. However, as interaction between the particles enhances, they often aggregate as early

*Paper based on a presentation at the 2nd International Conference on Green Chemistry (ICGC-2), 14–20 September 2008, Moscow, Russia. Other presentations are published in this issue, pp. 1961–2129.

‡Corresponding author

as the structure formation stage and governed changes in aggregation of nanocarbons under treatment. Such interaction could result in new properties of materials produced from the nanocarbons and unpredictable environmental effect of carbon nanoparticles [1]. The ultradisperse systems formed are metastable, and it is, therefore, important to develop conditions under which they could be kept stable for a long time. The structure and dynamics of formation of a nanoscale carbon net can be described by comparative study of different fullerene-like particles because they are morphologically and genetically similar.

The problem is particularly acute for a new generation of carbonaceous materials because they have a highly developed surface and reactivity. Fullerene-like particles, such as nanotubes, onion structures, and ultradisperse diamonds (UDDs), are promising materials for the development of nanotechnologies. Biomedical application is the most challenging as long as carbon nanoparticles become available in the form of stable dispersions in water [2,3]. Water plays the role of a disperse medium and a regulator of intermolecular interactions among carbon nanoparticles, and can also play an important part in the production of new composite materials from fullerene-like nanoparticles because its evaporation gives rise to considerable cohesive forces that can substantially increase the durability and chemical resistance of the carbon networks produced. Microdynamic properties of molecules of water in the vicinity of nanocarbons as well as the contribution of hydration to the structural and morphological characteristics and stability of nanocarbon complexes are the subject of intensive study [4,5].

Numerous pathways have been employed for the synthesis of carbon nanoparticles with different morphologies as well as size distribution. Most of these proceed via high energy and further purification by wet methods with the use of highly reactive agents that are not environmentally friendly.

Here the main attention is concentrated on two different forms of nanocarbon particles that could be combined by the way of their green synthesis, namely, through stable aqueous dispersion without any additives. In conjunction with using water for releasing the carbon nanoparticles from shungite carbon (ShC) and UDD materials, it is worth a reminder that there are at least two more aspects concerning these materials from the point of view of "green chemistry". First of all, ShC is originated from natural carbonaceous shungite rocks, otherwise crude detonation nanodiamond is being produced on an industrial scale from military explosives [(mixture of TNT($C_7H_5N_3O_6$)-hexogen ($C_3H_6N_6O_6$)] using the expired or overproduced stocks as the raw material.

It is challenging to compare nanocarbons of different origin that could be stabilized in water without using surfactants. The aim of the present paper was to study a low-temperature ozone oxidation of synthetic UDD and natural ShC in terms of their structure and physicochemical properties.

ULTRADISPERSE DIAMOND

UDD powders produced by the detonation synthesis have the potential to achieve truly widespread use [6]. Development of most applications is hindered because of poor reproducibility of properties of UDD even from the same producer. In order to eliminate the differences, liquid-phase purification (wet chemistry) as well as dry chemistry including catalyst-assisted oxidation, ozone-enriched, and air oxidation was used [7]. Surface properties and size distribution pattern are changed at every stage of UDD treatment.

Usually, UDDs could be characterized by a two-level pattern. Thus, each UDD particle occurs as a monocrystalline diamond core (4–5 nm) surrounded by a graphene shell, which is responsible for the chemical state of the UDD surface [8]. In the initial powder, nanoparticles form tight aggregates, their particle size being >200 nm. To release primary particles, special treatment of the initial UDD powder in water in a stirred-media milling with zirconia microbeads was applied. As a result, stable aqueous dispersion with UDD particles, ~5 nm in size, is formed, as supported by dynamic light-scattering (DLS) and transmission electron microscopy (TEM) data [9]. Small-angle neutron scattering (SANS) experiments, conducted using contrast variation on UDD dispersions in different liquids (water, DMSO, and ethanol), have shown that primary UDD particles are typically ~6 nm in size and form aggregates

whose volumetric fractal size is ca. 2.3 [10]. The narrow size distribution of primary particles is one of the remarkable assets of monodisperse single nanodiamond particulates (*mdsn*-D) [11]. Among the behaviors of *mdsn*-D particles should be mentioned a remarkably high tendency to aggregate and great hygroscopicity. Gel formation from aqueous colloid of *mdsn*-D suggests strong hydration on the particle surface. It was obtained by differential scanning calorimetry (DSC). A nonfreezing endothermic peak at –8 °C in addition to the freezing peak of bulk water at 0 °C was revealed. The thickness of nonfreezing water layer is about 1 nm [12]. Specific nanocarbon–water interaction might be a reason for high stability of colloidal particles of *mdsn*-D in water. The question is under study now.

Shungite nanocarbon

Nanodimensional globules (<6 nm) were shown to be characteristic elements that make up the ShC matrix and were responsible for the properties of the natural carbon [13]. ShC globules are 3-dimensional closed, multilayered graphite shells that cover nanodimensional pores [14,15]. Structurally similar shungites from different deposits differ in morphology and useful properties such as porosity and specific surface [16]. Variations in the physicochemical properties of natural ShC and carbon-rich shungite rocks were reproduced in the laboratory by modifying of less active varieties of shungite. Determining the optimal activation conditions of the nanostructural elements of shungite rocks is an essential task for their efficient use as adsorbents, catalysts, and fillers of composite materials, both special types (to shield electromagnetic radiation) and multipurpose types [17].

An important stage in the formation of a nanodimensional system and its hierarchical structure is the initial stage at which globular aggregates are formed upon drying of aqueous ShC dispersions. It should be noted that nanoparticles, similar in size and nanoparticle distribution pattern, were revealed earlier on the fracture surfaces of pristine shungite samples, as corroborated by tunneling electron microscopy and atomic force microscopy (AFM) [18,19].

SANS data, obtained using contrast variation on shungite from different deposits (generated under different conditions: temperature, pressure, fluid composition), display a complex structural pattern over the size range 1–100 nm. Two structural levels are distinguished for all samples. Level I (characteristic particle radius >100 nm) corresponds to the structural units of ShC observed under AFM. Smaller particles (characteristic particle radius <10 nm), corresponding to structural level II, contribute to a mixture of open pores, accessible to absorbed molecules (D_2O), and closed pores inaccessible to the substances. The effect of the open to closed porosity ratio on SANS data correlates with Brunauer–Emmett–Teller (BET) adsorption data.

Pores on level II have an internal fractal structure built by particles whose sizes are beyond the resolution limits of the SANS experiment, ~1 nm. The particles are considered to be a basic (minimum) structural unit (BSU) of ShC [20]. The size of the latter, estimated earlier by small-angle X-ray scattering (SAXS) and high-resolution (HR)-TEM is 0.5–0.7 nm [15,16]. Such elements could be easily transformed into water. Study of ShC stable aqueous dispersion by high-resolution, solid-state ^{13}C and ^{1}H MAS NMR, and time-of-flight mass spectrometry enables us to determine the bowl shape (nonplanar graphene layers) and characteristic mass ~284 m/z of BSU [21].

Modification

Practically all carbonaceous materials, used as adsorbents, catalysts, and fillers for industrial purposes, are preactivated by high-temperature treatment in an oxidizing or reducing medium. As a result, porosity and specific surface area increase and the composition of functional surface groups changes. The negative result of such an activation is the loss of a considerable amount of initial carbon and, what is fairly essential, the inability to control the process. These problems can be avoided by the low-temperature ozonization method [22].

As ShC and *mdsn*-D particles have a similar herarchical structure organization, namely, a two-level structural pattern, and curved graphene shells or their fragments contribute to the formation of the structure and surface properties of both ShC and *mdsn*-D particles, a comparative study of the effect of ozonization on the physicochemical properties of these ultradisperse naturally and synthetically generated carbonaceous materials was conducted.

EXPERIMENTAL SECTION

Shungite powders were produced by grinding on a vibrating mill to a particle size less than 40 μm of samples (carbon content 98 wt %) picked out at Shunga and Nigozero deposits, characterized thoroughly elsewhere [15,20,23] were studied. Carbon from Shunga is characterized by low porosity and surface area. It was used as the initial ShC in preparation of aqueous dispersions. The carbon from Nigozero was supposed to originate in hydrothermal conditions from shungite of Shunga.

Aqueous dispersion was prepared from the powder using ultrasonic treatment, filtration, and centrifugation as described in [24]. The ShC dispersion was dried at room temperature in vacuum until carbon particles precipitated. An average particle size detected by TEM in the precipitated ShC dispersion was 10–100 nm, AFM and SEM showed aggregates with an average size 62 nm.

UDD was produced by Gansu Liru Lingyun NanoMaterial Co., Ltd., Lanjou, China, by the detonation method. After drying concentrated aqueous dispersions, the diamonds were subjected to additional purification and ground in a stirred-media milling with zirconia beads less than 30 μm in diameter to produce *mdsn*-D as described in detail elsewhere [11].

Oxidation of ShC and *mdsn*-D samples by ozone was carried out at flow rate 5 l/h and 20 °C. Ozone was synthesized under barrier electrical discharge from oxygen (high purity). Ozone content in the mixture was 2–5 vol %.

Concentration of oxygen-containing groups (OGs) was measured by titration method and analyzing of FTIR spectra that were registered by Brucker EQUINOX 55/S spectrometer on pills with KBr (1:100).

Thermal gravimetry (TG) was conducted on a Netzsch Luxx 409 PC in a dynamic mode at an airflow of 50 ml/min. The sample was heated from room temperature to 1200 °C at a rate of 10°/min.

Electron paramagnetic resonance (EPR) spectra were obtained on a Bruker EMX-220 digital spectrometer at a frequency of 9.4 GHz with a sensitivity not lower than 10^{11} spin/G. The standard was sugar coal, 6×10^{16} spin/sample, intermediate standard (Cr^{3+} in corundum).

SAXS spectra were taken at CuK_{α} radiation. X-ray scatter was recorded on a D-Max-B/RC Rigaku Geigerflex diffractometer over the angle range 0.5–100. To correct for angle, diffraction patterns were taken in a wide-angle range. Calibration was done from the first quartz peak.

To study structural changes, electron microscopy images were produced in the transmission mode and diffraction images in the microdiffraction mode on an EM-125 electron microscope. Microdiffraction studies were carried out using TlCl standard.

The adsorption of molecules of different size, namely, dichloromethane (0.33 nm), benzene (0.37 nm), cyclohexane (0.48 nm), and water (0.28 nm) was used to monitor the evolution of microporosity of ShC and *mdsn*-D owing to ozonization. Measurements of these adsorptions were carried out by a static technique, using a gravimetric apparatus (McBain balance).

The sorption isotherms of nitrogen were obtained at 77 K with a standard commercial automatic device Quantachrome Instruments with Autosorb 1C analyzer. Samples were degassed at 323 K prior to every adsorption experiment. The isotherms of the other adsorbates were measured at 298 K and over the same relative pressure range. The densities of adsorbed species were assumed to be identical to those of the corresponding bulk liquids at the adsorption temperature. Pore distribution patterns were obtained based on Kelvin equation. Volume and radius of micropores were determined by the Dubinine–Radushkevitch (DR) equation as described elsewhere [25].

RESULTS

Ozonization kinetics

Figure 1 shows differential (a) kinetic curves for ozone absorption and CO_2 emission upon oxidation of ShC. Carbon oxide (II) is not detected. The kinetic curves are typical of fine-grained ShC oxidation: a rapid transition to a steady-state ozone consumption mode, ozone absorption being practically complete for all samples, and non-steady-state vibration kinetics for CO_2, unusual for oxidation of carbonaceous materials (Fig. 1a). Regular oscillations were related to periodical oxidation and reduction of the active surface layer of the carbon, whereas the aperiodicity of vibrations could be due to an intradiffusion retardation effect. The oscillations are more pronounced for fresh powders.

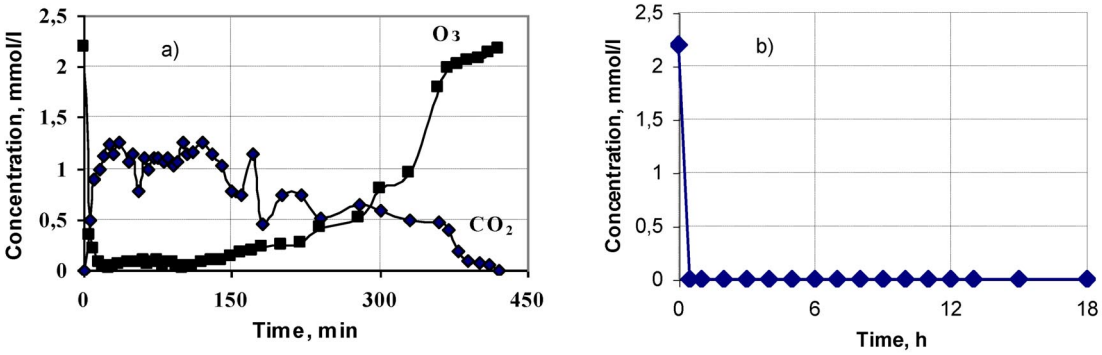

Fig. 1 Differential kinetic curves for ozone adsorption and CO_2 emission upon oxidation of ShC (a) and ND (b). Ozone was completely decomposed. No CO_2 was detected during the ozonization of ND.

In the case of ShC, the quantities of absorbed ozone and released CO_2 exceed the ratio expected for a deep oxidation reaction of carbon [22].

During *mdsn*-D ozonization, the dominant process is ozone decomposition, whereas CO_2 is virtually not released. It was assumed that 100 % decomposition of ozone into *mdsn*-D is actually associated with metal microimpurities, the oxides of which are capable of decomposing ozone. Nevertheless, the initial UDD that contains higher concentration of the impurities but larger tight aggregates showed only partial ozone decomposition.

The catalytic activity of *mdsn*-D is: 3.4×10^{18} molecules/s.g, which is higher by one order of magnitude than the value estimated for shungite in powder form, 2.4×10^{17} molecules/s.g [26].

ShC nanoparticles when released through water dispersions were established to accelerate ether thermal decomposition and tetralin dehydrogenation [27]. The results obtained suggest a special role of BSU in these processes, which could be due to a high concentration of free electrons on their surface (ozone decomposes on the donors of electrons). We suppose that such a high activity could be intrinsic to nanocarbons themselves.

Surface modification

Figure 2 shows the Fourier transform-infrared (FT-IR) spectra of initial and ozone-modified *mdsn*-D that can be used to trace the evolution of the functional surface cover. Similar ShC spectra are discussed in detail in [22]. Attention should first be drawn to the most intense absorption band at 1630 cm^{-1}, which belongs to the deformation oscillations of water and ceases to be asymmetrical after *mdsn*-D ozonization.

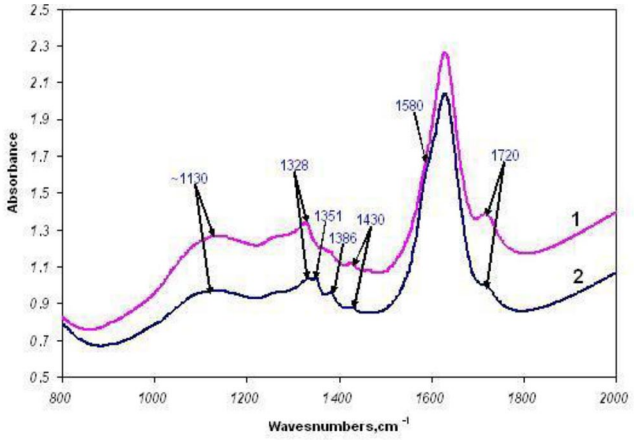

Fig. 2 IR spectra of initial (1) and ozonized *mdsn*-D (2).

The asymmetry of this absorption maximum is due to the fact that a system of conjugate >C=C< bonds, characteristic of graphitic structures, is overlapped with an intense absorption band at 1580 cm^{-1}. Another important evidence for a change in the *mdsn*-D sample upon ozonization is the complete disappearance of the absorption band at 1351 cm^{-1} and a marked weakening of the absorption maxima at 1430–1320 cm^{-1}. Located in this interval are medium-intensity absorption bands, corresponding to the deformation vibrations of the –>C–H– bonds of alkyl groups that have different electron surroundings. Thus, absorption at 1430 and 1350 cm^{-1} are characteristic of the methyl and methylene groups, respectively.

The maximum at 1720 cm^{-1} corresponds to the absorption of carbonyl groups. Its intensity in ozonized *mdsn*-D is observed to rise slightly, which was supported by a rise in concentration of OG by titration. A wide signal with a maximum at 1130 cm^{-1} is due to the superposition of the vibration of different molecular sites that include ether and peroxide groups.

The above evidence has led us to conclude that ozonization results in the selective purification of *mdsn*-D, represented by sp^3-hybrid carbon, from graphene impurities that form the shell of diamond nanoparticles.

Increasing in concentration of OG was observed by titration of initial and ozonized *mdsn*-D. Carboxyl groups were not detected on the surface of initial UDD, but their concentration increased up to 0.210 mg-eqv/g when ground in a stirred-media milling, and a further increase to 0.306 mg-eqv/g under ozonization was determined.

Unlike *mdsn*-D, ShC has a richer functional composition. The FT-IR spectrum of ShC is complicated by the vibrations of conjugate systems of multiple bonds that interact with carbonyl groups and C–H (at C) atoms of aromatic systems and a large number of peroxide and ether bonds. As a result of oxidative modification of ShC, its specific surface increases, and it is considerably enriched in carbonyl and especially ether groups. It has been assumed that ether bonds in ShC are included dominantly in epoxy cycles, which correlates with a marked weakening of the absorption bands of >C=C<– bonds after ozonization [22].

The differential EPR spectra obtained for the initial and ozonized *mdsn*-D are equally wide, 120 Hz. Only a small increase in line width was observed with a decline in temperature (77 K) for the initial and ozonized *mdsn*-D samples. Table 1 shows the results of processing of the EPR spectra of *mdsn*-D and those of ShC obtained earlier [26].

Table 1 EPR spectrum data for *mdsn*-D and ShC samples in vacuum.

Sample	Paramagnetic centers		*g*-factor
	Spin/g	Spin/m^2	
mdsn-D original	3.9×10^{19}	1.3×10^{17}	2.0025
mdsn-D ozonized	4.6×10^{19}	1.5×10^{17}	2.0026
ShC original	2.3×10^{19}	1.5×10^{18}	2.0019
ShC ozonized	2.2×10^{19}	3.4×10^{17}	2.0016

The results obtained are in good agreement with the *g*-factor values for *mdsn*-D, 2.0027 ± 0.0001, and the concentration of paramagnetic centers (PC), 10^{19}–10^{20} spin/g, published in [28]. As a result of *mdsn*-D ozonization by 8 and 14 %, the "surface" and "bulk" concentration of the PC, respectively, increase. The "bulk" concentration for ShC remains practically unchanged, whereas its "surface" concentration diminishes by virtue of an increase in the specific surface of ShC upon ozonization.

Releasing of active entities by ozonization

DSC-TG study has shown that for ShC a marked weight loss with a positive heat effect begins at 410 °C and ends at 800 °C. There are two maxima on the DSC curve: a maximum at 510 °C and a weak maximum at 645 °C (Fig. 3).

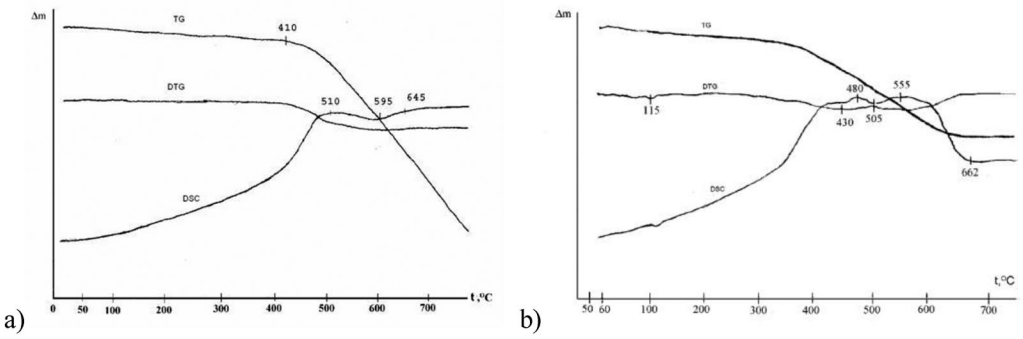

Fig. 3 TG of ShC (a) pristine, (b) ozonized.

For a ShC sample, ozonized for 9.5 h, a marked weight loss with a positive heat effect (carbon oxidation) begins at a lower temperature of 300 °C and ends at 670 °C. There are three maxima on the DSC curve: 430, 480, and 555 °C and a small minimum at 115 °C, which corresponds to water and CO_2 desorption. In the temperature range 660–820 °C no changes are observed. Three maxima that correspond to the formation of CO_2 at lower temperatures than for initial ShC, result from an increase in the degree of dispersity of ShC after ozonization.

The effect of released nanoparticles was detected for ShC converted into the form of aqueous dispersion. Two maxima at 501 and 585 °C for initial ShC powder transformed to the narrow peak at 450 °C of ShC nanoparticles in dispersion.

Analysis of the TG, differential thermal analysis (DTA), and DSC curves of the initial and ozonized *mdsn*-D samples (Fig. 4) shows: a slight increase in mass (1–1.9 %) at 397 °C, accompanied by an exothermal effect and associated presumably with the formation of OG on the *mdsn*-D surface. Burning of the carbon begins at a temperature of ~500 °C. The graphene shell is the first to burn out

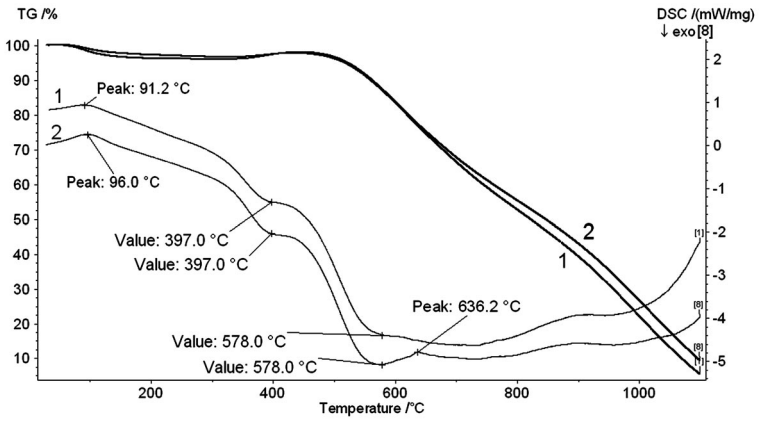

Fig. 4 TG of *mdsn*-D samples initial (1) and ozonized (2).

because the exothermal effect that we see in the case of the initial *mdsn*-D is absent in the ozonized sample (T = 578 °C).

Porosity

The ozonization of shungite powder has enabled the authors to reveal an increase in nanoporosity described by SANS on natural shungite [20]. Scatterers, structural elements, of three characteristic sizes: 2.6, 4.5–5.8, and 25.0–26.5 nm, were determined by SAXS (Table 2).

Table 2 Sizes of the structural elements of modified ShC estimated by the SAXS method.

Samples and treatments	Fractal dimension	BSU, nm	Size of the clusters, nm
Shungite (original)	2.20	0.51	4.5–6.0, 13.0; ≥30.2;
Shungite (ozonized)	2.19	0.51	0.39, 2.6, 4.5–5.8, 25.0–26.5
Film of ShC aqueous dispersion			7.7; >30.1

*BSU: minimal structural element.

The practically invariable fractal size value upon ozonization, D = 2.187 (initial D = 2.2), indicates the invariability of open porosity (Table 2). If scatterers are understood as pores, formed as a result of ozonization, then their sizes can be checked by adsorption methods.

Two minimum sizes are apparent on the diffraction patterns for all modified ShC samples: a small peak in the range $2\theta_{Br}$ = 13.23 deg. (0.389 nm) and 10.14 deg. (0.507 nm). Both peaks on the diffraction curve proved to be more pronounced on the ozonized ShC.

The particles of initial shungite powder typically are varying in size from 20 nm to over 2 μm and the parameters of electron diffraction patterns that agree with those of Shunga ShC [15]. Under TEM, the particles exhibit a fairly uniform contrast, suggesting their homogeneous surface relief and the absence of large pores.

Upon ozonization, the particle sizes actually remain unchanged, but the particles analyzed display a heterogeneous contrast, which is due to the emergence of porosity that varies in size from 20 to 50 nm (Fig. 5). In addition, the half-width values of diffraction peak I (002) increase, indicating a relative decrease in the size of the coherent scatter domains in the direction perpendicular to graphene layers and, accordingly, an increase in the size of structural ultramicroporosity (Table 3). Thus, the total surface in-

creases both at the expense of an increase in inner globular porosity and of the oxidation of some ShC domains that vary in size from 20 to 50 nm. These results are in good agreement with earlier adsorption data on an increase in the number of ultramicropores (~0.4 nm) and mesopores (10–50 nm) as a result of ShC ozonization [17].

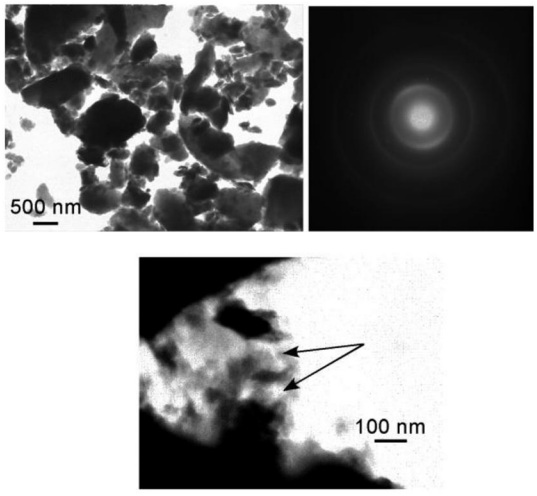

Fig. 5 Electron microscopic images of ozonized shungite powder and corresponding electron diffraction pattern of ozonized ShC. Arrows show pores appeared on ozonization varying in size from 20 to 50 nm.

Table 3 Interplanar distances and half-width of the diffraction maxima of ShC.

ShC original		ShC ozonized	
d_{002} (Å)	*FWHM*	d_{002} (Å)	*FWHM*
3.51	7.2	3.50	8.7
2.08	6	2.07	5.2
1.21	–	1.21	–

FWHM: apparent full width at half maximum.

Adsorption data

The use of adsorptives that vary in size has been recommended to assess the micropore size distribution of any microporous material due to the lack of a reliable procedure for its computation from a single isotherm [29]. An example of experimental nitrogen adsorption–desorption isotherms, obtained on *mdsn*-D and ShC, is shown in Fig. 6.

It can be seen that both samples are primarily mesoporous with a pronounced hysteresis in the desorption isotherm. The isotherms could be ascribed to type IV. A slight difference between hysteresis loops could be noticed. The loop on ShC is thus similar to the one of nonrigid adsorbents (Fig. 6a). The flexibility of pore walls could affect pore width: adsorption brings to increasing in pore width, while during desorption the pore size decreases. Similar effects were reported for chemically purified montmorillonites [30], whereas the isotherm obtained on *mdsn*-D is typical of porous bodies consisting of rigid spherical particles. The BET surface area is found to be 283.8 and 325.0 m^2/g for *mdsn*-D and ShC, respectively. The specific surface values of the samples are sensitive to the time and storage conditions of the powders.

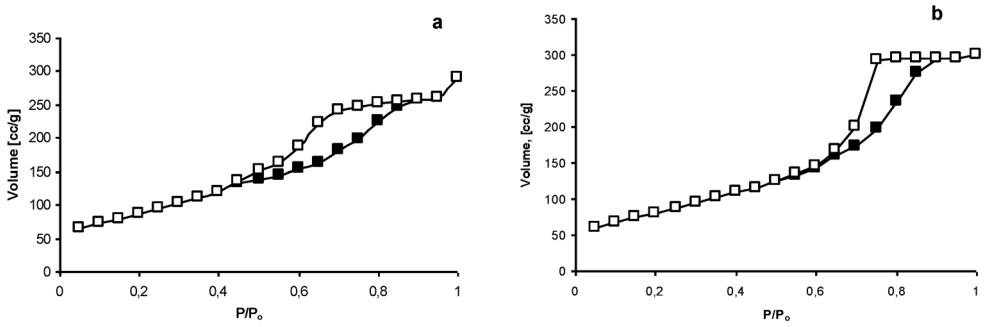

Fig. 6 Nitrogen adsorption–desorption isotherms at 77 K on ShC (a) and *mdsn*-D (b).

Analysis of adsorption isotherms of molecules of different size resulted in calculations of specific surface (S) and volume adsorption (V) data using DR and BET equation. They are presented in the Table 4. $V(CO_2, DR)$ could be attributed to the ultramicropore volume with effective pore widths H in the frames of the $0.33 < H < 0.7$ nm, while $V(N_2, DR)$ is often accepted as a measure of the total micropore volume ($H < 2$ nm). The so-called submicropore volume, which pore widths verify ($0.7 < H < 2$ nm), is thus given by the difference $V(N_2, DR) - V(CO_2, DR)$. The results obtained were analyzed and presented in graphs (Figs. 7 and 8).

Table 4 Specific surface and volume adsorption data of *mdsn*-D and ShC.

	H_2O		CO_2		CH_2Cl_2		C_6H_6		C_6H_{12}	
Samples, treatment	V, cm^3/g	S, m^2/g	V, cm^3/g	S, m^2/g	V, cm^3/g	S, m^2/g	V, cm^3/g	S, m^2/g	V, cm^3/g	S, m^2/g
mdsn-D	0.250	491.8	0.066	172.5	0.47	391.0	0.46	324.2	0.47	375.0
mdsn-D ozonized	0.280	503.2	0.063	164.7	0.48	399.7	0.48	340.3	0.48	402.0
ShC (Shunga)	0.10	200.3	0.033	87.7	0.035	52.7	0.03	15.7	0.03	29.3
ShC after dispersion	0.337	577.7	0.055	144.2	0.111	64.8	0.24	34.9	0.21	39.9

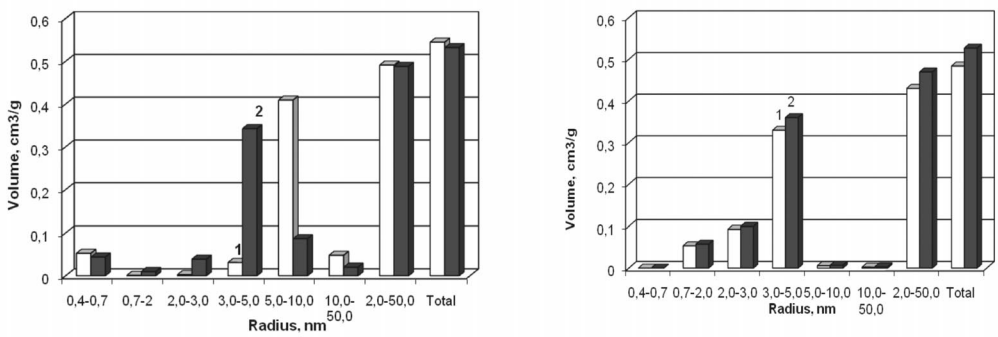

Fig. 7 Pore size distribution pattern of *mdsn*-D: (a) adsorption of C_6H_6 calculated for the split-like pores (1) and for the cylindrical-like pores (2); (b) char bar of pore size distribution pattern for *mdsn*-D untreated (1) and ozonized (2).

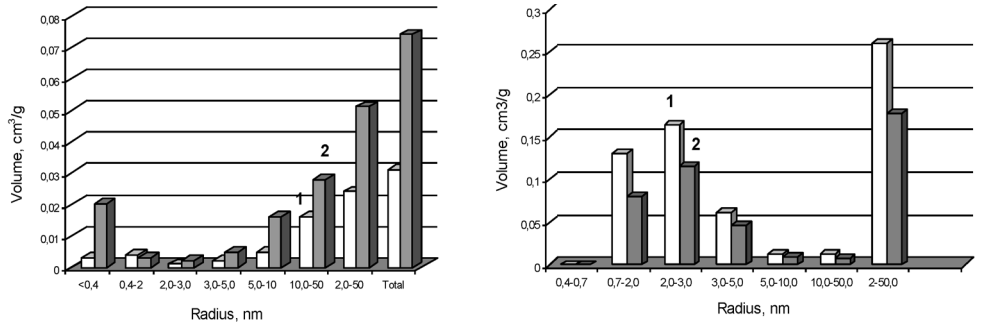

a b

Fig. 8 Pore size distribution pattern of ShC (Shunga) (a) and Nigozero (b): 1, initial; 2, ozonized.

The surface area of mesopores was determined from the desorption branch of the benzene isotherms, assuming the cylindrical or slit-like shape of the mesopores. The models description is given in [30]. Pore size distribution pattern was calculated, based on both models, as shown for *mdsn*-D in Fig. 7a. The split-like model fits better for mesopores 3–6 nm in size, while a cylindrical shape of pores is more preferable for the pore range 5–10 nm.

The largest total volume close to *mdsn*-D and released nanoparticles of ShC (nanoparticles from aqueous dispersion as well as from Nigozero) was established for nitrogen and water adsorption. Thus, the specific surface area of *mdsn*-D and ShC for water molecule adsorption is equal to 503.2 and 577.7 m^2/g, respectively (Table 4).

The *mdsn*-D sample exhibits a higher adsorption capacity than ShC for all probes. Ozonization does not strongly affect the adsorption volume as well as the surface area of *mdsn*-D. The pore size distribution pattern of *mdsn*-D did not change upon ozonization either (Fig. 7b). An average pore size is equal to 6.7 nm (Table 5).

Table 5 Adsorption parameters of *mdsn*-D and ShC on nitrogen adsorption.

Samples, treatment	S, m^2/g	V, cm^3/g at $p/p_0 = 0.95$	Average pore radius, nm	
			BET	DR method
mdsn-D	283.8	0.475 ($r < 39.7$ nm)	3.35	3.37
mdsn-D ozonized	306.2	0.516 ($r < 45.24$ nm)	3.37	3.45
ShC (Nigozero)	325.0	0.406 $r < 21.3$ nm	2.50	3.14
ShC (Nigozero) ozonized	204.9	0.257 $r < 22.0$ nm	2.51	3.13
ShC after dispersion	325.4	0.45		

Pristine ShC (Shunga) shows close adsorption volumes toward different molecules. It changes noticeably with releasing ShC structural units. Differences in the texture and adsorption properties of ShC and *mdsn*-D are clearly seen if the pore size distribution pattern presented in graphs (Figs. 7b, 8a) is

compared. The difference could be diminished when ShC nanoparticles are released through water dispersion (Fig. 8b).

Ozonization of ShC, as well as releasing of the nanoparticles, resulted in the development of its ultramicroporosity and mesoporosity (Fig. 8). Two average pore radius values, 3.1 and 2.5 nm, were determined for ShC (Nigozero) (Table 5).

CONCLUSIONS

The study of the ozonization kinetics of ShC and *mdsn*-D showed their high catalytic activity on ozone decomposition that entails elimination of the strong oxidizer concentration in the environment. Graphene fragments are assumed to contribute to the catalytic effect observed.

During *mdsn*-D ozonization under mild conditions (low temperatures), sp^2-hybrid carbon is removed selectively from the nanodiamond core surface, as supported by the results of FT-IR spectroscopy and derivatography.

Both electronic (concentration of paramagnetic centers) and surface properties (concentration of OGs) of *mdsn*-D are changed upon ozonization.

Unlike *mdsn*-D, ozonization of ShC results in changed structural parameters. For example, electron microscopy and electron diffraction data show a rise in structural porosity, which agrees with SAXS results: upon ozonization, fractal size does not change, whereas internal ultramicroporosity of 0.4–0.5 nm increases. These conclusions are supported by adsorption methods.

ShC and *mdsn*-D show well-developed mesoporosity. The average size of the pores is estimated at 6.7 and 6.1 nm for *mdsn*-D and ShC, respectively.

ShC nanoclusters, released through aqueous dispersion upon concentration, reproduce the adsorptive properties of active shungite (Nigozero) that was originated in hydrothermal conditions and approaches the adsorption capacity and specific surface values of *mdsn*-D.

ACKNOWLEDGMENTS

The authors would like to thank Dr. V. V. Kovalevski for performing TEM and SAED measurements, Dr. V. M. Senyavin for FT-IR experiments, and Drs. M. A. Yagovkina and V. I. Siklitski for SAXS measurements. The work was supported by SI-Visby-00996/2008, RFBR Grant 06-03-32446 (MVK), NEDO Grant, 2004IT081 (E. Ōsawa).

REFERENCES

1. H. W. Kroto, D. R. M. Walton (Eds.). *The Fullerenes: New Horizons for the Chemistry, Physics and Astrophysics of Carbon*, Cambridge University Press, Cambridge (1993).
2. S. Yamago, H. Tokuyama, E. Nakamura, K. Kikuchi, S. Kanaishi, K. Sueki, H. Nakahara, S. Enomoto, F. Ambe. *Chem. Biol*. **2**, 385 (1995).
3. H. Huang, E. Pierstorff, E. Ōsawa, D. Ho. *Nano Lett.* **7**, 3305 (2007).
4. M. Gordillo, G. Nagy, J. Marti. *J. Chem. Phys*. **117**, 3425 (2002).
5. T. Hotta, M. Sasai. *J. Phys. Chem. C* **111**, 2861 (2007).
6. O. A. Shenderova, G. McGuire. In *Nanocrystalline Diamond in Nanomaterials Handbook*, G. Yu (Ed.), pp. 203–237, CRC Press, Boca Raton (2006).
7. S. Osswald, G. Yushin, V. Mochalin, S. O. Kucheye, Yu. Gogotsi. *J. Am. Chem. Soc.* **128**, 11635 (2006).
8. A. Kruger, F. Kataoka, M. Ozawa, A. Aksenskii, A. Ya. Vul', Y. Fjino, A. Suzuki, E. Ōsawa. *Carbon* **43**, 1722 (2005).
9. E. Ōsawa. *Diamond Relat. Mater*. **16**, 2018 (2007).

10. M. V. Avdeev, N. N. Rozhkova, V. L. Aksenov, V. M. Garamus, R. Willumeit, E. Ōsawa. *J. Phys. Chem. C* **113**, 9473 (2009).
11. E. Ōsawa. *Pure Appl. Chem*. **80**, 1365 (2008).
12. M. V. Korobov, N. V. Avramenko, A. G. Bogachev, N. N. Rozhkova, E. Ōsawa. *J. Phys. Chem. C* **111**, 7330 (2007).
13. V. V. Kovalevski, N. N. Rozhkova, À. Z. Zaidenberg, A. N. Yermolin. *Mol. Mater.* **4**, 77 (1994).
14. À. Z. Zaidenberg, N. N. Rozhkova, V. V. Kovalevskii, D. C. Lorents, J. Chevallier. *Mol. Mater.* **8**, 107 (1996).
15. V. V. Kovalevski, P. R. Buseck, J. M. Cowley. *Carbon* **39**, 243 (2001).
16. N. N. Rozhkova, E. A. Golubev, V. I. Siklitsky, M. V. Baidakova. In *Fullerene and Fullerene-like Structures*, P. A. Vityaz' et al. (Eds.), pp. 100–107, ITMO BAS, Minsk (2005).
17. N. N. Rozhkova, G. I. Emel'yanova, L. E. Gorlenko, V. V. Lunin. *Russ. Chem. J.* **XLVIII**, 107 (2004).
18. N. N. Rozhkova. In *Perspectives of Fullerene Nanotechnology*, E. Ōsawa (Ed.), pp. 237–251, Kluwer Academic, Dordrecht (2002).
19. E. A. Golubev, N. N. Rozhkova, V. N. Filippov. *Surface* **10**, 47 (2007).
20. M. V. Avdeev, T. V. Tropin, V. L. Aksenov, L. Rosta, V. M. Garamus, N. N. Rozhkova. *Carbon* **44**, 54 (2006).
21. N. N. Rozhkova, A. V. Gribanov, M. A. Khodorkovskii. *Diamond Relat. Mater.* **16**, 2104 (2007).
22. G. I. Emel'yanova, L. E. Gorlenko, N. A. Tikhonov, N. N. Rozhkova, V. S. Rozhkova, V. V. Lunin. *Russ. J. Phys. Chem.* **78**, 1070 (2004).
23. A. Z. Zaidenberg, N. N. Rozhkova, V. V. Kovalevski, A. G. Tupolev. *Fullerene Sci. Technol.* **6**, 511 (1998).
24. S. P. Rozhkov, V. V. Kovalevski, N. N. Rozhkova. *Russ. J. Phys. Chem*. **81**, 1 (2007).
25. A. Jankowska, T. Siemieniewska, K. Tomków, M. Jasienko-Halat, J. Kaczmarczyk, A. Albiniak, J. J. Freeman, M. Yates. *Carbon* **31**, 871 (1993).
26. L. E. Gorlenko, G. I. Emel'yanova, N. A. Tikhonov, A. V. Fionov, N. N. Rozhkova, V. V. Lunin. *Russ. J. Phys. Chem*. **79**, 1232 (2005).
27. N. N. Rozhkova. Activation of Fullerene-like Structures in Shungite Carbon/Carbon'02. An International Conference, 15–19 September 2002, Beijing, China, program and short abstr., p. 81 (CD).
28. A. M. Panich, A. I. Shames, H.-M. Vieth, M. Takahashi, E. Ōsawa, A. Ya. Vul'. *Eur. J. Phys. B* **52**, 397 (2006).
29. J. Rouquerol, D. Avnir, C. W. Fairbridge, D. H. Everett, J. H. Haynes, N. Pernicone, J. D. F. Ramsay, K. S. W. Sing, K. K. Unger. *Pure Appl. Chem*. **66**, 1739 (1994).
30. S. J. Gregg, K. S. W. Sing. *Adsorption, Surface Area and Porosity*, 2nd ed., Academic Press, London (1982).